



Evaluation of surface roughness of novel Al-based MMCs using Box-Cox transformation

J. Nagendra¹ · M. K. Srinath¹ · G. Shaikshavali² · C. Labesh Kumar³ · Din Bandhu⁴ · Praveena Bindiganavile Anand⁵ · Santhosh Nagaraja⁶ · Ashish Saxena⁷

Received: 7 July 2023 / Accepted: 10 September 2023 / Published online: 25 October 2023
© The Author(s), under exclusive licence to Springer-Verlag France SAS, part of Springer Nature 2023

Abstract

Composites play a significant role in societal development. Therefore, the machining of composites is a significant topic of interest among the research community. In this context, this work uses stir-casted composite (Al-6061 alloy with graphene powder (5%), and nano-TiO₂ (10%)) as a workpiece. Depth of cut, cutting speed, and feed rate were considered significant factors at three levels. The experimental design was formulated based on Taguchi's design of experiment (DOE) and used an L₉ orthogonal array. The process's output characteristic was measured in terms of surface roughness (R_a) using a Surface Roughness Tester. The regression analysis has been applied to determine the best process parameters with little trial and error. The likelihood estimator (λ) was calculated using the Box-Cox transformation, yielding a powerful regression equation. The estimated values from the regression equation and the observed values were quite close to one another. A 0.687 R_a value was achieved with a 1 mm depth of cut, 1000 rpm spindle speed, and a 50 mm/min feed rate. To produce the smallest possible discrepancy between observed and anticipated values, the 'hyperparameter' of the regression equation was fine-tuned. The maximum likelihood estimator value of λ was found to be 2, with a mean error of 0.03%. The variance inflation factor was also found to be 1.00, which justifies the correctness of the equation.

Keywords Surface roughness · CNC parameter optimization · Taguchi analysis · Design of experiment · Maximum likelihood estimation · Box-Cox transformation

✉ Din Bandhu
din.bandhu@manipal.edu

¹ Department of Mechanical Engineering, New Horizon College of Engineering, Bangalore, Karnataka 560103, India

² Department of Mechanical Engineering, G. Pulla Reddy Engineering College (Autonomous), Kurnool, Andhra Pradesh 518007, India

³ Department of Mechanical Engineering, Institute of Aeronautical Engineering, Hyderabad, Telangana 500043, India

⁴ Department of Mechanical and Industrial Engineering, Manipal Institute of Technology Bengaluru, Manipal Academy of Higher Education, Manipal, Karnataka 576104, India

⁵ Department of Mechanical Engineering, Nitte Meenakshi Institute of Technology, Bangalore, Karnataka 560064, India

⁶ Department of Mechanical Engineering, M. V. J. College of Engineering, Bangalore, Karnataka 560067, India

⁷ School of Mechanical Engineering, Lovely Professional University, Phagwara, Punjab 144001, India

1 Introduction

Aluminium and its alloys commonly exhibit notable multi-property characteristics, including a high strength-to-weight ratio, excellent heat conductivity, and effective resistance against corrosion, under typical circumstances. As a consequence, these materials may be implemented across a wide range of industries. Notwithstanding their notable attributes, these materials have notable drawbacks like diminished mechanical strength, inadequate wear resistance, and subpar corrosion resistance when exposed to submerged water environments [1–4]. The utilization of aluminium-based metal matrix composites (MMCs) is a viable solution to mitigate these limitations. In order to acquire the requisite mechanical, physical, chemical, or thermal characteristics, metal matrix composites (MMCs) fundamentally amalgamate two or more components at the macroscopic level. They are widely utilized in many industries such as manufacturing electrical equipment, automotive, marine, and aerospace, owing to their distinctive characteristics [5–7]. Ceramic materials are

commonly employed as reinforcement in composites due to their ability to increase the essential characteristics of the composites [8–10]. The Al-6082 alloy (Si) is primarily composed of two prominent alloying elements, namely magnesium (Mg) and silicon. The alloy has moderate mechanical strength and high resistance to air corrosion. It is commonly utilized as a construction material for architectural elements necessitating substantial structural integrity, such as cranes, bridges, and trusses [11–13]. Likewise, Al-6061 is a widely recognized aluminium alloy renowned for its exceptional ratio of strength to weight, commendable resistance to corrosion, and favorable weldability. When the combination of titanium dioxide (TiO₂) and graphene is utilized, it introduces novel opportunities and augments its characteristics for diverse applications. Several uses of this material may be observed in various industries such as Aerospace and Aviation, Automotive Industry, Marine and Offshore Industries, Sports Equipment, Medical Devices, and other sectors [14–16].

To evaluate the performance efficiencies and mechanical properties of aluminium and aluminium-based matrix composites, numerous research-related activities and evaluations have been conducted [17–20]. The literature demonstrates that the creation of composite materials can enhance the hardness, wear, and corrosion characteristics of MMCs based on aluminium. By using ceramic components, aluminium composites were created. The results of the literature review revealed that adding ceramic components not only increased the composite's macro and micro hardness but also considerably increased its wear and corrosion resistance. The stir-casting procedure is one of the most used methods for creating composites. Ceramics made of Titanium Dioxide (TiO₂), and Graphene powder, which are tough, can be utilized as reinforcement for composite materials. Additionally, it has good qualities for resisting corrosion [21–23]. Researchers are actively working on research on the impacts of TiO₂ and graphene powder in composites for corrosion resistance and enhancing thermal and electrical conductivity. However, TiO₂ and graphene powder has a well-established history of usage as a hardening reinforcement, and it has been studied to determine the effect of produced metal composites on various properties [24–26]. With the use of SEM examination, the microstructure of the TiO₂ and Graphene powder-reinforced MMC is thoroughly examined. The results have revealed numerous modifications in the mechanical characteristics of TiO₂ and Graphene powder-enhanced MMCs [27–29]. This reinforcement has generally improved the mechanical properties of the produced composites, which is a good thing. According to studies, TiO₂ and Graphene powder has a more favourable impact on mechanical characteristics including hardness and compressive strength. Studies have revealed that the increased hardness of TiO₂ and Graphene powder reinforced

composites also enhances their tribological characteristics [30, 31]. According to research, TiO₂ and Graphene powder are largely utilized to enhance the mechanical and tribological characteristics of composite materials [32, 33].

It is necessary to investigate the extent of the post-processing technique's operational parameters [34–36]. The needed surface finish can be produced by choosing the correct operating parameter values. Numerous tests and testing of the specimens may be necessary due to the wide variation in the number of parameters and their range [37–39]. Taguchi-Design of experiments (T-DoE), an optimization technique, is used to get around this laborious process [40–42]. By using this technique, it is possible to identify the post-processing settings that are most effective at giving coated surfaces the desired surface finish [42–44]. Experimentation and surface roughness testing can be used to validate the optimal values. A surface coating with a high-quality surface finish is produced as a result of using the best post-processing settings [45–47].

The ideal values of the process parameters were obtained using optimization techniques. Researchers have used a variety of techniques for process parameter optimization, including turning of AISI 5140 for flank wear, cutting forces and vibration [48, 49], plasma arc cutting [50], welding of similar and dissimilar metals [51–54], fused filament fabrication for part geometry accuracy [55], dry sliding wear characteristics [56, 57], forming process [58], and cold rolling for improved surface characteristics [59]. According to the literature, a variety of methodologies can be used for process parameter optimization, however, Taguchi analysis is the most effective in terms of the outcomes.

In their study, Fang and Hong [60] explored various transformations of the response variable and subsequently developed estimation and confidence intervals for the resulting non-linear model's uncertainty. In the context of the Box-Cox model with general uncertainty, the utilization of the uncertain least squares method for estimation may result in a flawed estimate due to the transformation parameter approaching negative infinity and zero. This issue arises due to the tendency of the aforementioned parameters towards these limiting values. Liu et al. [61–63] proposed the rescaled least squares estimation (RLSE) method to obtain results for the uncertainty Box-Cox regression model. However, it should be noted that this method is only applicable to the Box-Cox transformation and cannot be used for a general uncertain model [64]. An alternative methodology is the uncertain maximum likelihood estimation (MLE), which has been proposed in recent literature. The authors Lio [61] and Liu [62] introduced the maximum likelihood estimation (MLE) approach for the continuous uncertainty model and implemented it in the context of the uncertainty linear regression model.

The present study aims to enhance the surface finish and minimize the surface roughness of the Al alloy composite subjected to turning operation by optimizing the CNC turning operating parameters. The optimization of operating parameters, namely Depth of Cut (DoC), Spindle Speed (SS), and Feed Rate (FR), will be carried out through the utilization of Taguchi analysis in combination with the Single-Response Performance Index (SPI). Acquiring the regression equation that is fine-tuned with hyperparameters to accurately predict the surface roughness at a high level. The nature of the data plot is heteroscedastic, indicating that the variables are unbiased.

The utilization of analysis of variance (ANOVA) is a prevalent method for optimizing process parameters since it aids in the creation of regression equations. The primary objective of this study is to enhance optimization by employing the Box-Cox transformation technique and determining the maximum likelihood value (λ) to assess statistical significance (P-value). Following this, the variance inflation factor (VIF) is calculated, which functions as a quantitative measure for evaluating the existence of multicollinearity in regression analysis.

2 Materials and methods

The composite material consists of the matrix material and the matrix material selected for this study was the aluminium alloy Al-6061. Of all the aluminium alloys, Al-6061 alloy offers the highest strength and ductility as well as outstanding machinability, good bearing, and wear characteristics. Additionally, it has a low weight, a good strength-to-weight

ratio, and great open-air corrosion resistance. The automobile, aerospace, and marine sectors all make extensive use of it. Its lack of mechanical strength restricts its application. In order to make the use of aluminium alloy in high-strength bearing applications in the automotive and aerospace sectors simpler, extensive research on the material has been done through the creation of MMCs [11]. The composition of Al-6061 is shown in Table 1, and its mechanical properties are shown in Table 2.

Based on the existing body of research, ongoing efforts are being made to develop metal matrix composites (MMCs) with aluminium as the primary constituent, with the aim of catering to a diverse array of applications. The utilization of titanium dioxide (TiO₂) as reinforcement has been proven to enhance the necessary strength [21]. Graphene powder (C) is also used as a reinforcement as it is a good conductor of electricity and a good conductor of heat, due to the presence of free electrons. Obtaining the hyperparameter-tuned regression equation that predicts the surface roughness with high-level accuracy. The data plot is to be heteroscedasticity in nature, so the variables are not biased [27]. The mechanical properties of reinforcements are shown in Table 3. A flow chart to express the research work is shown in Fig. 1.

2.1 CNC turning operation

The present investigation aims to explore the optimization of CNC turning operation parameters that influence the diminution of surface roughness and enhancement of surface finish in machined composites. Figure 2 depicts the workpiece mounted on the CNC machine for machining. The machining operations were carried out using the CNC lathe CLT100. This CNC machine is flatbed type, with a Fanuc emulated

Table 1 Composition of Al-6061

Element	Al	Mg	Si	Fe	Cu	Cr	Zn	Ti	Mn	Others
% by Wt (Minimum)	98.85	0.8	0.4	0	0.15	0.04	0	0	0	0
% by Wt (Maximum)	98.56	1.2	0.8	0.7	0.4	0.35	0.25	0.15	0.15	0.15

Table 2 Mechanical properties of Al-6061

Property	Density	Youngs modulus	Tensile strength	Percentage of elongation	Poisson's ratio
Magnitude	2.70 gm/cm ³	68 GPa	124–290 MPa	12–25%	0.33

Table 3 Mechanical properties of Titanium Dioxide and Graphene

Property	Density	Youngs modulus	Tensile strength	Poisson's ratio
TiO ₂	0.00397–0.00405 mg/m ³	230–288 GPa	333.3–367.5 MPa	0.27–0.29
Graphene (C)	2.25 gm/cm ³	2.4 TPa	130 GPa	0.19

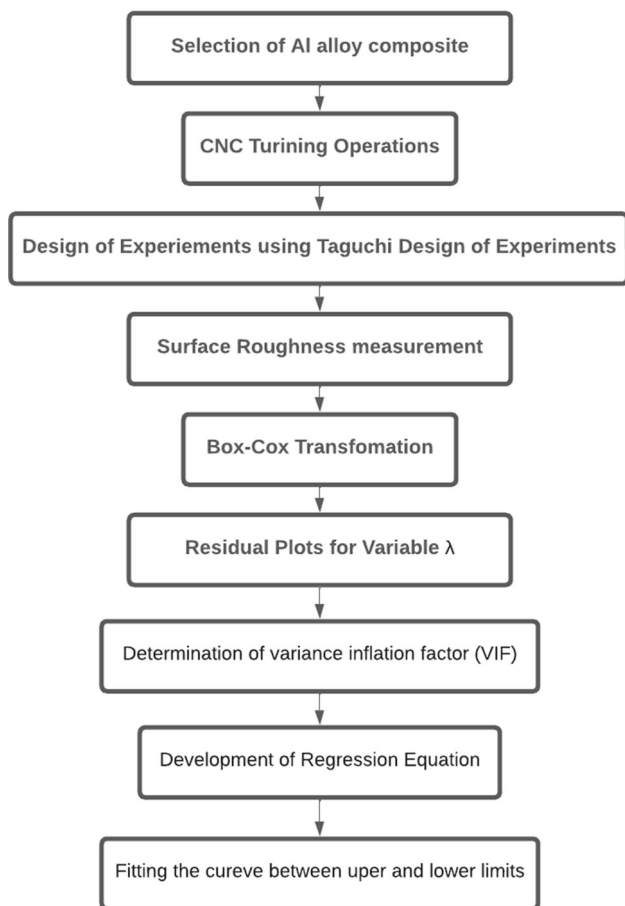


Fig. 1 Research study flowchart

keyboard. The chuck is manual with a maximum size of 100 mm dia. The CNC controller is ‘Cutviewer’, operating software which is a PLC-based controlled system. The CNC machine is automatic with a stepper motor with stepper drives. The Taguchi analysis was utilized together with

the Single-Response Performance Index (SPI) to optimize the Depth of Cut (DoC), Spindle Speed (SS), and Feed Rate (FR) operating parameters. The optimization of operating parameters was carried out to achieve the desired surface finish.

2.2 Design of experiments using Taguchi method (T-DoE)

The turning process parameters of the CNC lathe must be optimized in order to improve the surface quality finish of composite materials. The present investigation involved the utilization of Taguchi analysis for the optimization of process parameters. Figure 3 depicts the flow chart of the Taguchi Design.

During the preliminary phase, the T-DoE methodology relies on the number of process parameters associated with turning operations and the number of levels at which each of these factors is evaluated. Table 4 depicts the process parameters and their respective levels for the turning operation, which have been determined in accordance with the capacity of the CNC machine that has been selected for the purposes of this investigation.

The determination of the optimal combination of process parameters for turning operations, which results in the minimum surface roughness (R_a), is contingent upon the number of parameters and their respective levels. The present investigation involved the consideration of three distinct process parameters, each with six corresponding levels. Equation 1 [59] was utilized to establish the required number of trials.

$$\text{No. of Experiments} = P \times (L - 1) + 1 \quad (1)$$

where L depicts levels and P represents parameters.

The present investigation utilized the T-DoE methodology and determined that a total of 9 experimental trials have been

Fig. 2 CNC Turning tool and specimen

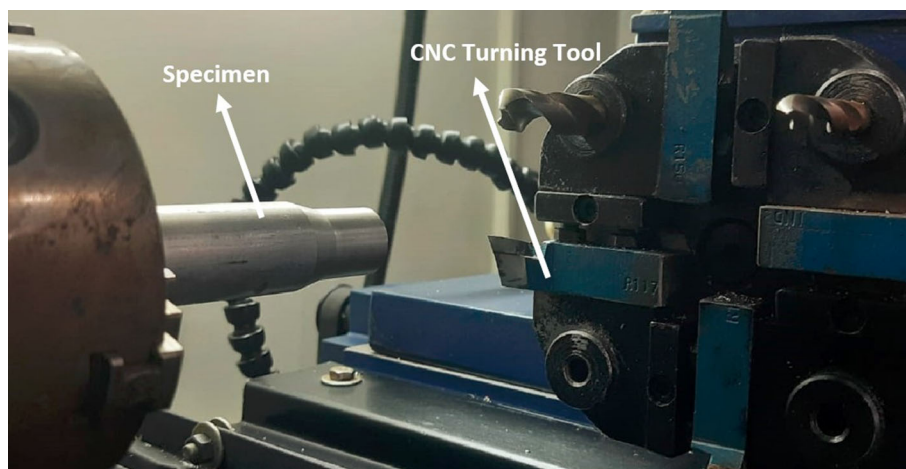


Fig. 3 T-DoE flow chart

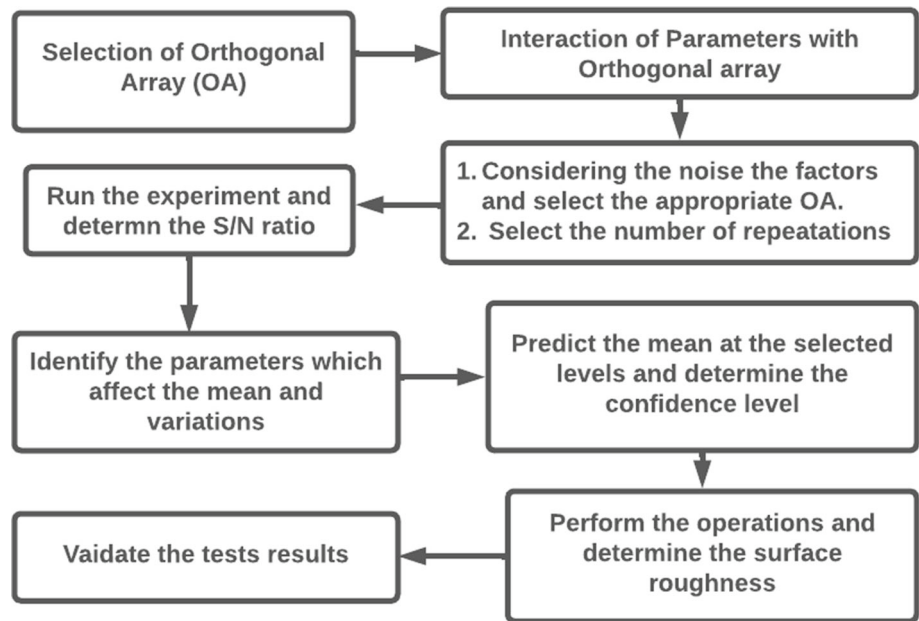


Table 4 CNC Turning Operation Process Parameters and their Levels

Operating process parameters		Depth of cut	Spindle speed	Feed rate
Units		(mm/cycle)	(rpm)	(mm/min)
Assigned variables		A	B	C
Magnitudes	Level- 1	1.0	1000	50
	Level- 2	2.0	2000	75
	Level- 3	3.0	3000	100

Table 5 Turning operation process parameters and their levels

Trail no	Depth of cut (mm/cycle)	Spindle speed (rpm)	Feed rate (mm/min)
1	1	1000	50
2	1	2000	75
3	1	3000	100
4	2	1000	75
5	2	2000	100
6	2	3000	50
7	3	1000	100
8	3	2000	50
9	3	3000	75

necessary. Orthogonal arrays of L_9 and L_{27} are the available options in the T-DoE, of which L_9 is chosen as shown in Table 5. The experimental design involved the consideration of two replications in each run, with the response being determined as the average of the two replications.

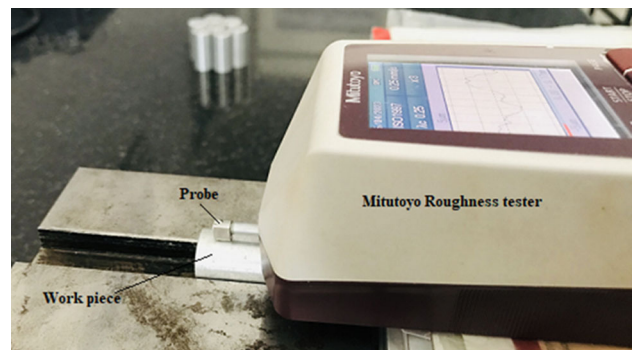


Fig. 4 Setup for measuring the surface roughness

2.3 Experimental setup and result measurement

The machining operation was conducted using a single-point cutting tool on a CNC turning centre. A rudimentary program for text conversion has been created with the aim of scholarly investigation. The surface roughness test was conducted using the Mitutoyo roughness tester as shown in Fig. 4. The other components for the surface roughness tests include the test specimen and an anvil. The specimen is kept over the

Table 6 Experimental Results with signal to noise ratio data

Trial no	Depth of cut (mm/cycle)	Spindle speed (rpm)	Feed rate (mm/min)	Surface Roughness (R_a)	SNR
1	1	1000	50	0.687	3.26087
2	1	2000	75	0.876	1.14992
3	1	3000	100	1.17	− 1.36372
4	2	1000	75	1.09	− 0.74853
5	2	2000	100	1.23	− 1.79810
6	2	3000	50	1.45	− 3.22736
7	3	1000	100	1.33	− 2.47703
8	3	2000	50	1.55	− 3.80663
9	3	3000	75	1.67	− 4.45433

v-groove of the anvil so that the lateral degrees of movement are arrested. The probe is set to be in contact with the workpiece and the probe movement was along the length of the workpiece. The measured results were recorded as presented in Table 6. Signal to noise ratio was calculated by using a smaller-is-better condition.

3 Results and discussion

By applying the 'smaller is better' criterion to the signal-to-noise ratio of the experimental findings, the influence of noise has been identified. The results of the signal-to-noise ratio (SNR) are presented in Table 6 along with the respective surface roughness values. The main effects plot of SRN is shown in Fig. 5. The significant combination of parameters identified from the experimental studies using the L_9 orthogonal array was the DoC = 1 mm/cycle, SS measured 1000 rpm, and FR of 50 mm/min. The plot was obtained from the Minitab platform. The surface roughness values constantly increased as and when the DoC, SS, and FR were raised. This could be due to the built-up edges at the cutting edge of the single-point HSS tool.

3.1 Mathematical modelling

For the mathematical modelling, a three-step process is used. The Box-Cox transformation and calculation of the maximum likelihood value (λ) for statistical significance (P-value) are described in detail in the first step [65–67]. The variance inflation factor (VIF), a metric for evaluating the presence of multi-collinearity in regression analysis, is determined in the second step [68–70]. The general linear regression is discussed in the third phase.

3.1.1 Box-Cox transformation

The utilization of the Box-Cox transformation methodology within the field of machine learning is implemented in order to achieve a normal distribution of the coefficients. The variable that is influenced by the independent variable is commonly represented as Y , while the variable that is being manipulated or controlled is typically denoted as $X = (1, x_1, x_2, x_3, \dots, x_k)$ [71]. The Box-Cox technique presents a model that facilitates the transformation of a non-normal distribution of data for variables A, B, and C, without reliance on the original scale. This method aims to achieve a normal distribution of the data [72].

$$Y_{BC}(Y, \lambda) = X\beta + \sigma e \quad (2)$$

where,

$$\text{If } \lambda \neq 0$$

$$Y_{BC}(Y, \lambda) = Y^\lambda - 1 \quad (3)$$

$$\text{If } \lambda = 0$$

$$Y_{BC}(Y, \lambda) = \text{Log}(Y) \quad (4)$$

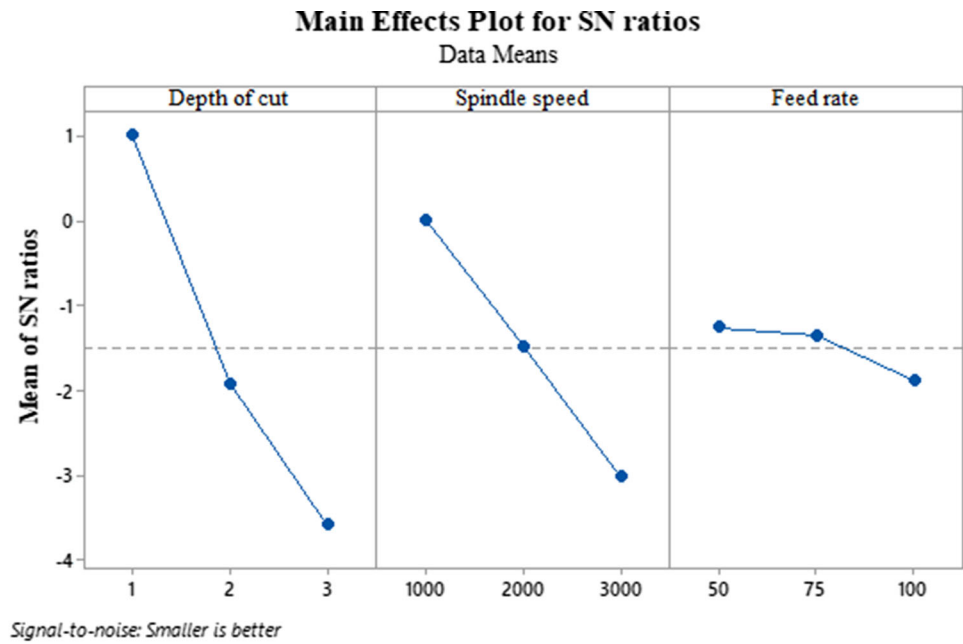
X is the covariate matrix including intercept.

$\beta = (\beta_0, \beta_1, \beta_2, \dots, \beta_k) =$ vector of regression coefficients.

The random error's variance is denoted by the symbol σ . The stochastic error term "e" follows the norm of the standard distribution. The Box-Cox transformation is used in Eq. 3, where the logarithm of Y reflects a particular case in which λ equals zero.

For estimating the parameter λ , the method of maximum likelihood is frequently used [73]. Multiple λ values are used to apply the model to the altered data; the best λ is then chosen since it produces the highest

Fig. 5 Main effect plot of Signal noise ratio



likelihood value. The fact that changing the covariates alters the likelihood value is one problem with this approach. The lambda argument will change as a result. Thus, the use of Minitab software to optimize the value in order to handle this problem was considered since it effectively uses the fit statistic approach. Equation (2) and Eq. (3) only apply to positive numbers, namely when Y is greater than 0. The Yeo-Johnson distribution family should be used when the dataset contains negative values since it can be used without placing any restrictions on the response variable (including negative replies). The ideal lambda value can be easily calculated in Minitab software to improve the correlation between the variables. This improves the equation’s accuracy as well [74].

The coefficient values for the intercept (constant), DoC, SS, and FR are displayed in Table 7. On either side of the scale, the values are evenly dispersed [62]. A negative number denotes the coefficients’ direction.

Figure 6(a) and (b) depict the pattern of the coefficient values. The values are much closer to the mean, which reflects the tuning of the model is proceeding in the right direction [61]. Both positive and negative correlations were noticed in the coefficient plot. Figure 6(a) represents the lambda value of 3. Figure 6(b) depicts the p-value trend for different values of lambda.

Figure 6(a) and (b) shows the coefficient plot for the variables as shown in Table 8. It was noticed that the coefficients were decreasing with the λ value reaching the optimum value. This signifies that the model is highly accurate and more significant [63]. The residual plot for all the lambda values is shown in Fig. 7(a), (b), (c), and (d).

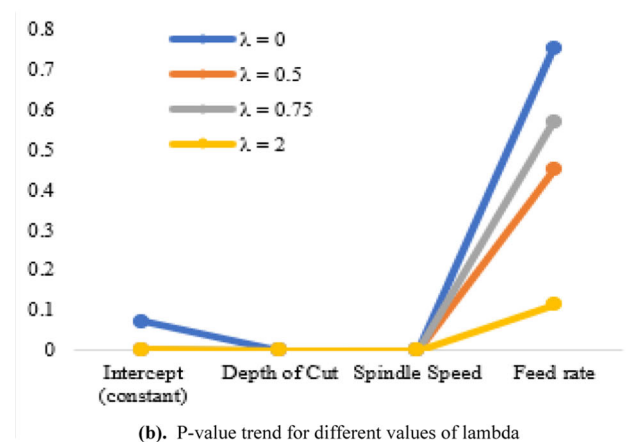
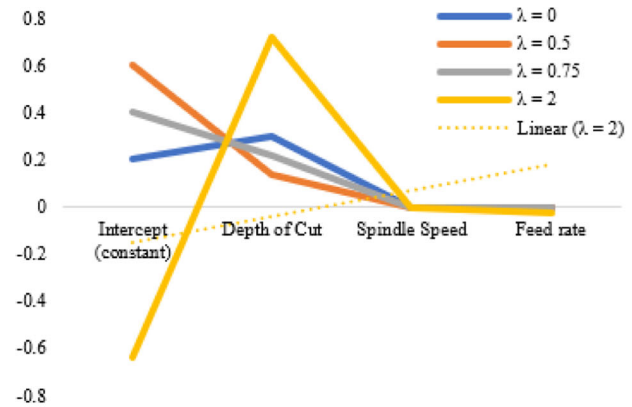


Fig. 6 Coefficient values and their P-value trend. a Coefficient values of the variables. b P-value trend for different values of lambda

Table 7 Coefficient values for different λ (hyper-parameter) value

Parameters	$\lambda = 0$	$\lambda = 0.5$	$\lambda = 0.75$	$\lambda = 2$ (Optimum)
Intercept (constant)	0.2066	0.6010	0.4042	- 0.634
Depth of cut	0.3028	0.1407	0.2186	0.7253
Spindle speed	0.000917	0.000092	0.000143	0.000472
Feed rate	0.000287	0.000440	0.000442	- 0.0218

Table 8 P-values for different λ (hyper-parameter) value

Parameters	$\lambda = 0$	$\lambda = 0.5$	$\lambda = 0.75$	$\lambda = 2$ (Optimum)
Intercept (constant)	0.071	0.0	0.003	0.003
Depth of cut	0.0	0.0	0.0	0.0
Spindle speed	0.0	0.001	0.001	0.0
Feed rate	0.753	0.450	0.569	0.114

Histogram in the residual plot shows the frequency distribution. The histogram [Fig. 7 (d)] for the λ value of 2.0, is distributed uniformly across both sides partially. Although the histogram is not perfect it is still within the acceptable range. Heteroscedasticity data was noticed in the verses fit, which is a clear sign of being unbiased. The linearity in the normal probability plot passes over all the residual points with minimum error, which is also a good fit. A two-way residual distribution was observed in the versus order.

3.1.2 Variance inflation factor

Variance Inflation Factor (VIF) determines the strength of the correlation between the independent variables. It is predicted by taking a variable and regressing it against every other variable. The R^2 value is determined to find out how well an independent variable is described by the other independent variables. A high value of R^2 means that the variable is highly correlated with the other variables [68, 69, 75]. This is captured by the VIF, denoted by the Equation,

The Variance Inflation Factor (VIF) is a statistical measure used to assess the degree of correlation among independent variables. Performing a regression analysis of a variable against all other variables results in the prediction. The R^2 value is utilized to assess the degree to which one independent variable is explained by the remaining independent variables. A strong correlation between a variable and its peers is indicated by a high R^2 [65, 66, 76]. The aforementioned concept is quantified by the Variance Inflation Factor (VIF), represented by the following equation:

$$VIF = \frac{1}{1 - R^2} \tag{5}$$

If the VIF value is lesser than 5, then the model is said to have low multicollinearity between the independent variables. Similarly, if the VIF value is between 5 to 10, then the

model has high collinearity, and the variables can be further tuned to fit the data. However, if the VIF value is above 10, it is removed or deleted from the data set as they are highly multicollinear. As shown in Table 9, the regression model exhibits the VIF value to be lesser than 5, which indicates that the factors are acceptable.

3.1.3 Linear regression

The regression equation denotes the statistical association between different independent variables and a response variable. Equation 5 represents the general regression equation.

$$Y = \beta_0 + \beta_1(A) + \beta_2(B) + \beta_3(C) \tag{6}$$

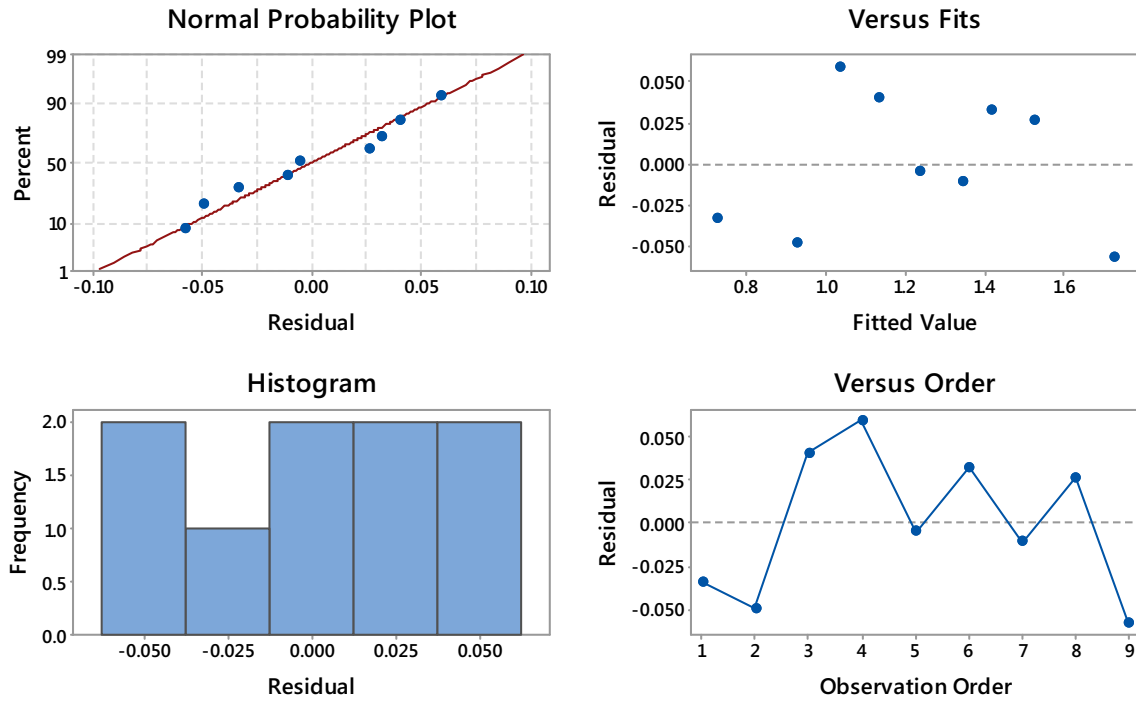
The aforementioned equation pertains to a linear regression model where Y represents the response variable, which in this case is surface roughness. β_0 denotes the intercept or constant, while β_1 , β_2 , and β_3 are the regression coefficients. The independent variables in question are denoted as "DoC," "SS," and "FR," represented by the letters A, B, and C, respectively. The linear regression equations for the variable 'Surface Roughness (SR)' were derived and expressed as Eqs. 6, 7, 8, and 9 for the lambda values of 0, 0.5, 0.75, and 2.0.

$$SR = 0.2066 + 0.3028(DC) + 0.000197(SS) + 0.000287(FR) \tag{7}$$

$$SR^{0.5} = 0.6010 + 0.1407(DC) + 0.000092(SS) + 0.000440(FR) \tag{8}$$

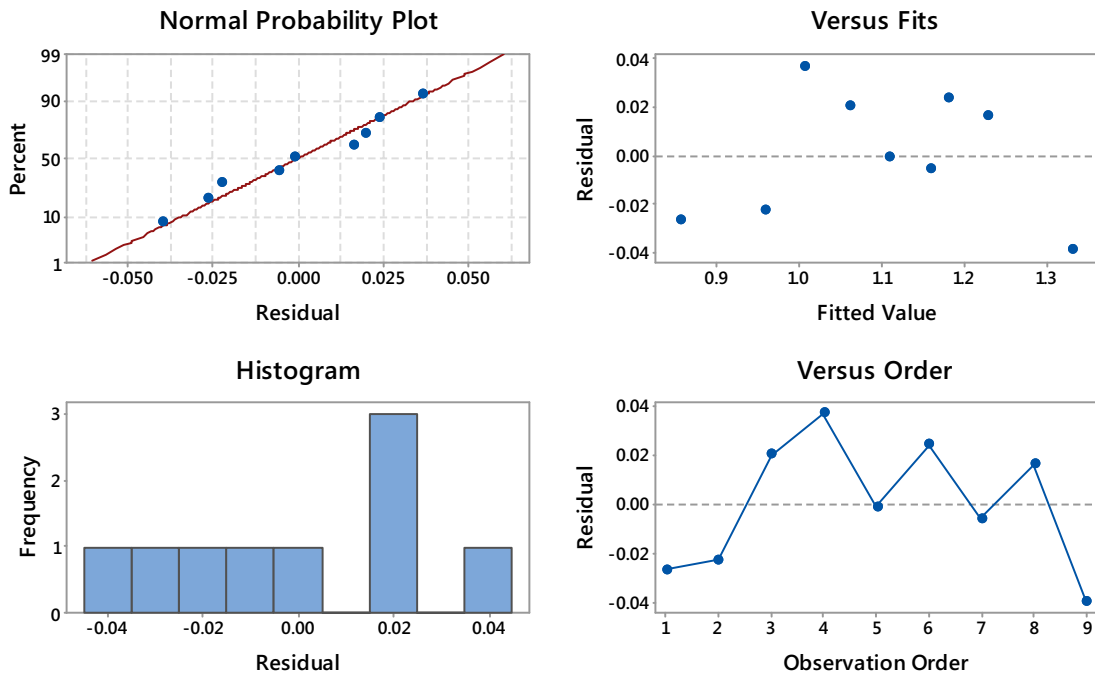
$$SR^{0.75} = 0.4042 + 0.2186(DC) + 0.000143(SS) + 0.000442(FR) \tag{9}$$

Residual Plots for Surf_roughness



(a). Residual plot of the variables $\lambda = 0.0$

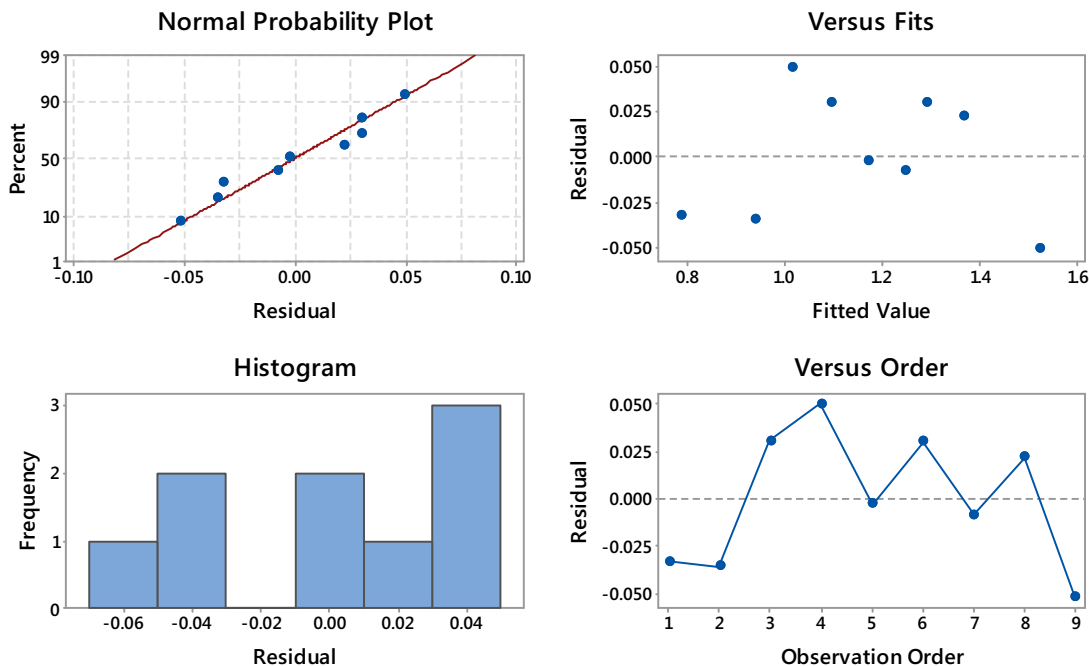
Residual Plots for Surf_roughness



(b). Residual plot of the variables $\lambda = 0.5$

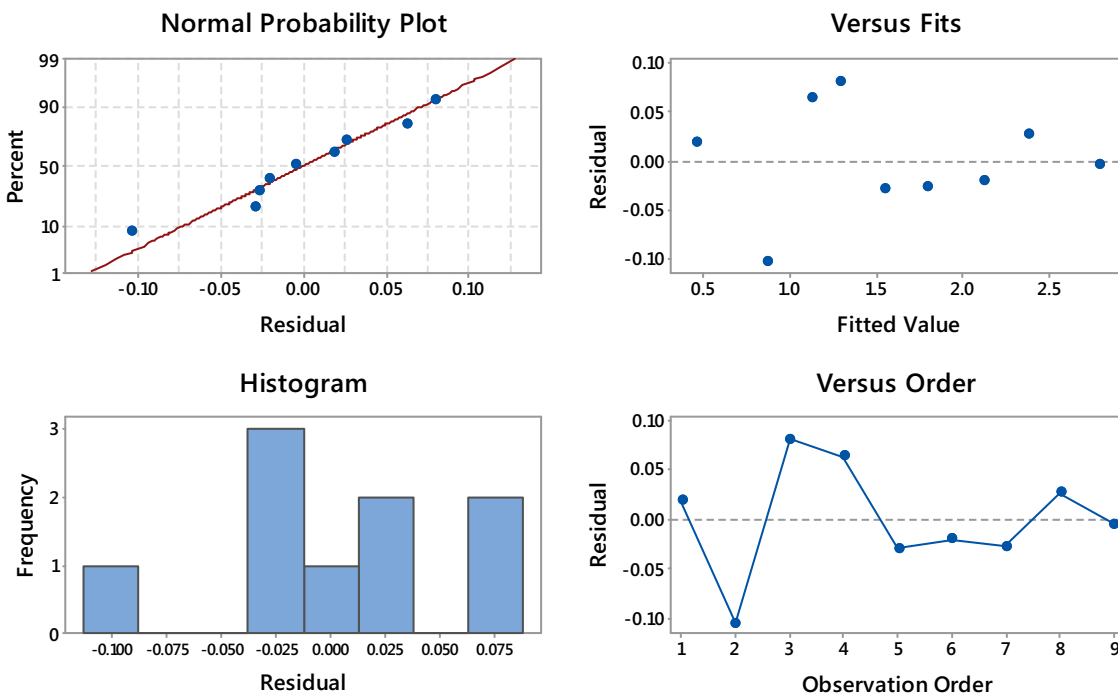
Fig. 7 Residual plots. **a** Residual plot of the variables $\lambda = 0.0$. **b** Residual plot of the variables $\lambda = 0.5$. **c** Residual plot of the variables $\lambda = 0.75$. **d** Residual plot of the variables $\lambda = 2.0$

Residual Plots for Surf_roughness



(c). Residual plot of the variables $\lambda = 0.75$

Residual Plots for Surf_roughness



(d). Residual plot of the variables $\lambda = 2.0$

Fig. 7 continued

Table 9 Variance Inflation Factor

Parameters	$\lambda = 0$	$\lambda = 0.5$	$\lambda = 0.75$	$\lambda = 2$ (Optimum)
Intercept (constant)				
Depth of Cut	1.00	1.00	1.00	1.00
Spindle Speed	1.00	1.00	1.00	1.00
Feed rate	1.00	1.00	1.00	1.00

Table 10 Experimental and predicted Surface roughness value with defined boundaries using 95% CI

Exp No	Depth of cut (mm)	Spindle Speed (rpm)	Feed rate	Experimental R_a (μm)	Predicted R_a (μm)	Upper limit R_a (μm)	Lower Limit R_a (μm)
1	1	1000	50	0.687	0.674	0.560	0.771
2	1	2000	75	0.876	0.934	0.882	0.983
3	1	3000	100	1.170	1.135	1.072	1.195
4	2	1000	75	1.090	1.061	1.015	1.104
5	2	2000	100	1.230	1.242	1.203	1.279
6	2	3000	50	1.450	1.457	1.416	1.498
7	3	1000	100	1.330	1.340	1.287	1.391
8	3	2000	50	1.550	1.542	1.502	1.580
9	3	3000	75	1.670	1.672	1.635	1.707

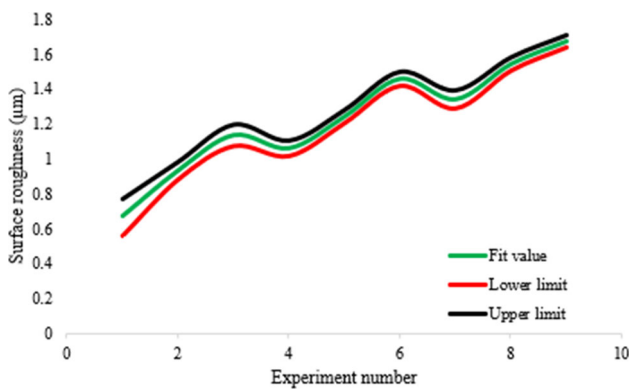


Fig. 8 Predicted value between upper and lower limit

$$SR^2 = -0.634 + 0.7253(DC) + 0.000472(SS) - 0.00218(FR) \tag{10}$$

The model summary of the predicted values is expressed in Table 6. The surface roughness values predicted after substituting in Eq. (7) are very much close to the actual experimental values and also well within the defined upper limit and lower limit. The predicted surface roughness values are fitted by assuming a 95% Confidence Interval (CI) for each variable. Table 10 displays the surface roughness values that were obtained through experimentation and prediction, while also taking into account defined boundaries and a 95% confidence interval. The graphical representation in Fig. 8 depicts

the predicted value of surface roughness within the range of the upper and lower limits.

4 Conclusions

The experimental process parameter combination is done by Taguchi design of experiment. L_9 Orthogonal array was selected, and the experimental combinations were framed by using Minitab. The predicted surface roughness was very much aligned with experimental results. This high-level accuracy was able to be established only after optimizing the hyperparameter lambda (λ). The following conclusions are drawn:

- The optimum λ value = 2 was determined using the box-cox transformation machine learning technique. This equation was further used for experimental data validation. Using a Bix-Cox transformation and an optimal lambda value can help improve the performance of statistical models and enhance the validity of their predictions or estimations, particularly when the assumptions of those models are violated due to skewed or non-normal data distributions. By applying the Box-Cox transformation with the optimal λ value of 2, improved performance was achieved in the statistical model and enhanced the validity of its predictions or estimations. This transformation

effectively addressed any issues related to skewed or non-normal data distributions, allowing the statistical model to make more accurate predictions and estimations.

- The coefficients also have equal contributions and were not biased. This proves that the regression equation built by using the optimum lambda value using box-cox transformation techniques has higher accuracy and high-reliability confidence. This approach of using the Box-Cox transformation technique with the optimal lambda value has not only enhanced the accuracy of the regression model but has also boosted its reliability and confidence. This demonstrates the effectiveness of experimental design, data preprocessing, and model-building processes.
- Obtained regression equation (Eq. 9) had a mean error of 0.03%, which was closer to the measured value. Having a mean error of only 0.03% in the obtained regression equation is a remarkable realization. A low mean error indicates that the predictions made by the regression model are very close to the actual measured values. This level of accuracy is desirable and suggests that your regression model is performing exceptionally well in capturing the relationships between the predictors and the response variable.

Funding The authors state there was no outside financing.

Data availability The authors confirm that the data supporting the findings of this study are available within the article.

Declarations

Conflict of interest The authors confirm that they have no competing interests with any third parties.

References

- Ozturk, K., Gecu, R., Karaaslan, A.: Microstructure, wear and corrosion characteristics of multiple-reinforced (SiC–B4C–Al₂O₃) Al matrix composites produced by liquid metal infiltration. *Ceram. Int.* **47**, 18274–18285 (2021). <https://doi.org/10.1016/J.CERAMINT.2021.03.147>
- Joshua, T.O., Alaneme, K.K., Bodunrin, M.O., Omotoyinbo, J.A.: Corrosion and wear characteristics of Al–Zn based composites reinforced with martensitic stainless steel and silicon carbide particulates. *Mater. Today Proc.* **62**, S127–S132 (2022). <https://doi.org/10.1016/J.MATPR.2022.02.099>
- Sharma, S.K., Saxena, K.K., Malik, V., Mohammed, K.A., Prakash, C., Buddhi, D., Dixit, S.: Significance of alloying elements on the mechanical characteristics of Mg-based materials for biomedical applications. *Crystals* **12**(8), 1138 (2022). <https://doi.org/10.3390/CRYST12081138>
- Thakur, A., Bandhu, D., Peshwe, D.R., Mahajan, Y.Y., Saxena, K.K., Eldin, S.M.: Appearance of reinforcement, interfacial product, heterogeneous nucleant and grain refiner of MgAl₂O₄ in aluminium metal matrix composites. *J. Mater. Res. Technol.* (2023). <https://doi.org/10.1016/J.JMRT.2023.07.121>
- Canakci, A., Ozkaya, S., Erdemir, F., Karabacak, A.H., Celebi, M.: Effects of Fe–Al intermetallic compounds on the wear and corrosion performances of AA2024/316L SS metal/metal composites. *J. Alloys Compd.* **845**, 156236 (2020). <https://doi.org/10.1016/J.JALLCOM.2020.156236>
- Murali Mohan, M., Venugopal Goud, E., Deva Kumar, M.L.S., Kumar, V., Kumar, M., Dinbandhu: Parametric optimization and evaluation of machining performance for aluminium-based hybrid composite using utility-taguchi approach. In: *Lecture Notes in Mechanical Engineering*, pp. 289–300. Springer, Singapore (2021).
- Sastry, M.N., Devi, K.D., Bandhu, D.: Characterization of *Aegle Marmelos* fiber reinforced composite. *Int J Eng Res* **5**(SP2), 345–49 (2016)
- Kalantarrashidi, N., Alizadeh, M.: Structure, wear and corrosion characterizations of Al/20wt.% Zn multilayered composites fabricated by cross-accumulative roll bonding. *J. Manuf. Process* **56**, 1050–1058 (2020). <https://doi.org/10.1016/J.JMAPRO.2020.05.023>
- Agarwal, K.M., Tyagi, R.K., Saxena, V., Choubey, K.K.: Mechanical behaviour of aluminium alloy AA6063 processed through ECAP with optimum die design parameters. *Adv. Mater. Process Technol.* **9**, 1901–1915 (2021). <https://doi.org/10.1080/2374068X.2021.1878705>
- Mehta, A., Vasudev, H., Singh, S., Prakash, C., Saxena, K.K., Linul, E., Buddhi, D., Xu, J.: Processing and advancements in the development of thermal barrier coatings: a review. *Coatings* **12**(9), 1318 (2022). <https://doi.org/10.3390/COATINGS12091318>
- Adin, H., Adin, M.S: Effect of particles on tensile and bending properties of jute epoxy composites. *Mater. Test.* **64**, 401–411 (2022). <https://doi.org/10.1515/MT-2021-2038/MACHINEREADABLECITATION/RIS>
- Awasthi, A., Saxena, K.K., Arun, V.: Sustainable and smart metal forming manufacturing process. *Mater. Today Proc.* **44**, 2069–2079 (2021). <https://doi.org/10.1016/J.MATPR.2020.12.177>
- Basanth Kumar, K., Saxena, K.K., Dey, S.R., Pancholi, V., Bhattacharjee, A.: Peak stress studies of hot compressed TiHy 600 alloy. *Mater. Today Proc.* **4**, 7365–7374 (2017). <https://doi.org/10.1016/J.MATPR.2017.07.066>
- Akinwande, A.A., Adediran, A.A., Balogun, O.A., Yibowei, M.E., Barnabas, A.A., Talabi, H.K., Olorunfemi, B.J.: Optimization of selected casting parameters on the mechanical behaviour of Al 6061/glass powder composites. *Heliyon* **8**, e09350 (2022). <https://doi.org/10.1016/J.HELIYON.2022.E09350>
- Awate, P.P., Barve, S.B.: Enhanced microstructure and mechanical properties of Al6061 alloy via graphene nanoplates reinforcement fabricated by stir casting. *Funct. Compos. Struct.* **4**, 015005 (2022). <https://doi.org/10.1088/2631-6331/AC586D>
- Atchudan, R., Edison, T.N.J.I., Mani, S., Perumal, S., Vinodh, R., Thirunavukkarasu, S., Lee, Y.R.: Facile synthesis of a novel nitrogen-doped carbon dot adorned zinc oxide composite for photodegradation of methylene blue. *Dalt. Trans.* **49**, 17725–17736 (2020). <https://doi.org/10.1039/D0DT02756A>
- Dhanalaxmi, B., Apparao Naidu, G., Anuradha, K.: Adaptive PSO based association rule mining technique for software defect classification using ANN. *Procedia. Comput. Sci.* **46**, 432–442 (2015). <https://doi.org/10.1016/J.PROCS.2015.02.041>
- Budarapu, P.R., Sudhir Sastry, Y.B., Natarajan, R.: Design concepts of an aircraft wing: composite and morphing airfoil with auxetic structures. *Front. Struct. Civ. Eng.* **10**, 394–408 (2016). <https://doi.org/10.1007/s11709-016-0352-z>
- Krishnaja, D., Cheepu, M., Venkateswarlu, D.: A review of research progress on dissimilar laser weld-brazing of automotive applications. In: *IOP Conference Series: Materials Science and Engineering*, p. 012073. IOP Publishing (2018). <https://doi.org/10.1088/1757-899X/330/1/012073>

20. Kota, V.R., Bhukya, M.N.: A novel global MPP tracking scheme based on shading pattern identification using artificial neural networks for photovoltaic power generation during partial shaded condition. *IET Renew. Power Gener.* **13**, 1647–1659 (2019). <https://doi.org/10.1049/IET-RPG.2018.5142>
21. Lin, T.H., An, H., Nam, N.T., Hai, N.D., Binh, T.L., Cong, C.Q., Huy, N.L., Buu, T.T., Minh, D.T., Phong, M.T., Hieu, N.H.: Magnesium ferrite/titanium dioxide/reduced graphene oxide composite photocatalyst for degradation of crystal violet under ultraviolet irradiation. *Mater. Chem. Phys.* **1**(301), 127661 (2023). <https://doi.org/10.1016/J.MATCHEMPHYS.2023.127661>
22. Peddakrishna, S., Khan, T.: Design of UWB monopole antenna with dual notched band characteristics by using π -shaped slot and EBG resonator. *AEU – Int. J. Electron. Commun.* **96**, 107–112 (2018). <https://doi.org/10.1016/J.AEUE.2018.09.014>
23. Chandrappa, V., Basavapoorima, C., Kesavulu, C.R., Babu, A.M., Depuru, S.R., Jayasankar, C.K.: Spectral studies of Dy³⁺: zincphosphate glasses for white light source emission applications: a comparative study. *J. Non Cryst. Solids* **583**, 121466 (2022). <https://doi.org/10.1016/J.JNONCRY SOL.2022.121466>
24. Arya, A., Iqbal, M., Tanwar, S., Sharma, A., Sharma, A.L., Kumar, V.: Mesoporous carbon/titanium dioxide composite as an electrode for symmetric/asymmetric solid-state supercapacitors. *Mater. Sci. Eng. B* **285**, 115972 (2022). <https://doi.org/10.1016/J.MSEB.2022.115972>
25. Godavarthi, B., Nalajala, P., Ganapuram, V.: Design and implementation of vehicle navigation system in urban environments using internet of things (Iot). *IOP Conf. Ser. Mater. Sci. Eng.* **225**, 012262 (2017). <https://doi.org/10.1088/1757-899X/225/1/012262>
26. Bhukya, M.N., Kota, V.R., Depuru, S.R.: A simple, efficient, and novel standalone photovoltaic inverter configuration with reduced harmonic distortion. *IEEE Access.* **7**, 43831–43845 (2019). <https://doi.org/10.1109/ACCESS.2019.2902979>
27. Krzywiński, K., Sieradzki, A., Sadowski, Ł., Królicka, A., Chastre, C.: Thermal wear of epoxy composite modified with rutile titanium dioxide. *Compos. Struct.* **282**, 115127 (2022). <https://doi.org/10.1016/J.COMPSTRUCT.2021.115127>
28. Budarapu, P.R., Yb, S.S., Javvaji, B., Mahapatra, D.R.: Vibration analysis of multi-walled carbon nanotubes embedded in elastic medium. *Front. Struct. Civ. Eng.* **8**, 151–159 (2014). <https://doi.org/10.1007/S11709-014-0247-9/METRICS>
29. Jaffery, H.A., Sabri, M.F., Said, S.M., Hasan, S.W., Sajid, I.H., Nordin, N.I., Hasnan, M.M., Shawah, D.A., Moorthy, C.V.: Electrochemical corrosion behavior of Sn-0.7 Cu solder alloy with the addition of bismuth and iron. *J. Alloy Compounds.* **25**(810), 151925 (2019). <https://doi.org/10.1016/J.JALLCOM.2019.151925>
30. Gupta, T.K., Budarapu, P.R., Chappidi, S.R., Paggi, M., Bordas, S.P.: Advances in carbon based nanomaterials for bio-medical applications. *Curr. Med. Chem.* **26**(38), 6851–77 (2019)
31. Korpi, A.G., Țălu, Ș., Bramowicz, M., Arman, A., Kulesza, S., Psczolkowski, B., Jurečka, S., Mardani, M., Luna, C., Balashabadi, P., Rezaee, S., Gopikishan, S.: Minkowski functional characterization and fractal analysis of surfaces of titanium nitride films. *Mater. Res. Express.* **6**, 086463 (2019). <https://doi.org/10.1088/2053-1591/AB26BE>
32. Yadav, S., Sharma, P., Yamasani, P., Minaev, S., Kumar, S.: A prototype micro-thermoelectric power generator for micro-electromechanical systems. *Appl. Phys. Lett.* (2014). <https://doi.org/10.1063/1.4870260/24501>
33. Balguri, P.K., Samuel, D.G.H., Thumu, U.: A review on mechanical properties of epoxy nanocomposites. *Mater. Today Proceed.* (2021). <https://doi.org/10.1016/j.matpr.2020.09.742>
34. Sun, G., Zhuang, S., Jia, D., Pan, X., Sun, Y., Tu, F., Lu, M.: Facile fabricating titanium/graphene composite with enhanced conductivity. *Mater. Lett.* **333**, 133680 (2023). <https://doi.org/10.1016/J.MATLET.2022.133680>
35. Jha, P., Shaikshavali, G., Shankar, M.G., Ram, M.D.S., Bandhu, D., Saxena, K.K., Buddhi, D., Agrawal, M.K.: A hybrid ensemble learning model for evaluating the surface roughness of AZ91 alloy during the end milling operation. *Surf. Rev. Lett.* (2022). <https://doi.org/10.1142/S0218625X23400012>
36. Jayanthi, N., Babu, B.V., Rao, N.S.: Survey on clinical prediction models for diabetes prediction. *J. Big Data.* **4**, 1–15 (2017). <https://doi.org/10.1186/S40537-017-0082-7/TABLES/7>
37. Numan, A., Gill, A.A., Rafique, S., Guduri, M., Zhan, Y., Maddiboyina, B., Li, L., Singh, S., Dang, N.N.: Rationally engineered nanosensors: a novel strategy for the detection of heavy metal ions in the environment. *J. Hazard. Mater.* **5**(409), 124493 (2021). <https://doi.org/10.1016/J.JHAZMAT.2020.124493>
38. Pratyush Reddy, K.S., Roopa, Y.M., Kovvada Rajeev, L.N., Nandan, N.S.: IoT based smart agriculture using machine learning. *Int. Conf. Inven. Res. Comput. Appl. ICIRCA* **2020**, 130–134 (2020). <https://doi.org/10.1109/ICIRCA48905.2020.9183373>
39. Vijayakumar, Y., Nagaraju, P., Yaragani, V., Parne, S.R., Awwad, N.S., Ramana Reddy, M.V.: Nanostructured Al and Fe co-doped ZnO thin films for enhanced ammonia detection. *Phys. B Condens. Matter.* **581**, 411976 (2020). <https://doi.org/10.1016/J.PHYSB.2019.411976>
40. Zuo, T., Wang, M., Xue, J., Ru, Y., Wu, Y., Ding, F., Da, B., Xu, Z., Liaw, P.K., Gao, Z., Han, L., Xiao, L.: Investigation on the novel copper-based composite conductors synergistically improved by in-situ generated graphene and nanoparticles. *Mater. Charact.* **200**, 112863 (2023). <https://doi.org/10.1016/J.MATCHAR.2023.112863>
41. Hamit, A.D., Yildiz, B., Adin, M.Ş.: Numerical investigation of fatigue behaviours of non-patched and patched aluminium pipes. *Eur. J. Tech. (EJT)*. **11**(1), 60–5 (2021)
42. Adin, M.Ş.: Performances of cryo-treated and untreated cutting tools in machining of AA7075 aerospace aluminium alloy. *Eur. Mech. Sci.* **7**(2), 70–81 (2023)
43. Safina, L.R., Krylova, K.A., Baimova, J.A.: Molecular dynamics study of the mechanical properties and deformation behavior of graphene/metal composites. *Mater. Today Phys.* **28**, 100851 (2022). <https://doi.org/10.1016/J.MTPHYS.2022.100851>
44. Bhukya, M.N., Kota, V.R.: A quick and effective MPPT scheme for solar power generation during dynamic weather and partial shaded conditions. *Eng. Sci. Technol. Int. J.* **22**, 869–884 (2019). <https://doi.org/10.1016/J.JESTCH.2019.01.015>
45. Wang, H., Zhang, H., Hao, S., Bi, Y., Jiang, W., Liu, J.: Preparation of SiC/multilayer graphene composite ceramic with improved properties catalyzed by Ni nanoparticle. *Ceram. Int.* **49**, 13836–13851 (2023). <https://doi.org/10.1016/J.CERAMINT.2022.12.263>
46. Adin, M.Ş.: A parametric study on the mechanical properties of MIG and TIG welded dissimilar steel joints. *J. Adhes. Sci. Technol.* (2023). <https://doi.org/10.1080/01694243.2023.2221391>
47. Rachid, H.B., Noureddine, D., Benali, B., Mehmet, &, Adin, Ş., S, UKR U Adin, M.: Effect of nanocomposites rate on the crack propagation in the adhesive of single lap joint subjected to tension. *Mech Adv Mater Struct.* (2023). <https://doi.org/10.1080/15376494.2023.2240319>
48. Suresh, A., Diwakar, G.: Optimization of process parameters in plasma arc cutting for TWIP steel plates. *Mater. Today Proc.* **38**, 2417–2424 (2021). <https://doi.org/10.1016/J.MATPR.2020.07.383>
49. Adin, M.Ş., İşcan, B.: Optimization of process parameters of medium carbon steel joints joined by MIG welding using Taguchi method. *Eur. Mech. Sci.* **6**(1), 17–26 (2022)

50. Behera, A.: Optimization of process parameters in laser welding of dissimilar materials. *Mater. Today Proc.* **33**, 5765–5769 (2020). <https://doi.org/10.1016/J.MATPR.2020.07.148>
51. Nath, P., Olson, J.D., Mahadevan, S., Lee, Y.T.T.: Optimization of fused filament fabrication process parameters under uncertainty to maximize part geometry accuracy. *Addit. Manuf.* **35**, 101331 (2020). <https://doi.org/10.1016/J.ADDMA.2020.101331>
52. Yadav, G.P., Bandhu, D., Krishna, B.V., Gupta, N., Jha, P., Vora, J.J., Mishra, S., Saxena, K.K., Salem, K.H., Abdullaev, S.S.: Exploring the potential of metal-cored filler wire in gas metal arc welding for ASME SA387-Gr. 11-Cl. 2 steel joints. *J. Adhesion Sci. Technol.* **15**, 1–22 (2023)
53. Bandhu, D., Vora, J.J., Das, S., Thakur, A., Kumari, S., Abhishek, K., Sastry, M.N.: Experimental study on application of gas metal arc welding based regulated metal deposition technique for low alloy steel. *Mater. Manuf. Process.* **37**, 1–19 (2022). <https://doi.org/10.1080/10426914.2022.2049298>
54. Dinbandhu, V.P., Vora, J.J., Abhishek, K.: Advances in gas metal arc welding process: modifications in short-circuiting transfer mode. *Adv. Weld. Deform.* **17**, 67–104 (2021). <https://doi.org/10.1016/b978-0-12-822049-8.00003-7>
55. Nagendra, J., Srinath, M.K., Sujeeth, S., Naresh, K.S., Ganesh Prasad, M.S.: Optimization of process parameters and evaluation of surface roughness for 3D printed nylon-aramid composite. *Mater. Today Proc.* **44**, 674–682 (2021). <https://doi.org/10.1016/J.MATPR.2020.10.609>
56. Aslan, A.: Optimization and analysis of process parameters for flank wear, cutting forces and vibration in turning of AISI 5140: a comprehensive study. *Measurement* **163**, 107959 (2020). <https://doi.org/10.1016/J.MEASUREMENT.2020.107959>
57. Nagendra, J., Prasad, M.S.G., Shashank, S., Ali, S.M.: Comparison of tribological behavior of nylon aramid polymer composite fabricated by fused deposition modeling and injection molding process. *Int. J. Mech. Eng. Technol.* **9**, 720–728 (2018)
58. Prabhu, P.R., Kulkarni, S.M., Sharma, S.: Multi-response optimization of the turn-assisted deep cold rolling process parameters for enhanced surface characteristics and residual stress of AISI 4140 steel shafts. *J. Mater. Res. Technol.* **9**, 11402–11423 (2020). <https://doi.org/10.1016/J.JMRT.2020.08.025>
59. Srinath, M.K., Nagendra, J.: Post-processing parameter optimization to enhance the surface finish of HVOF-developed coatings. *Multiscale Multidiscip Model Exp. Des.* **5**, 255–267 (2022). <https://doi.org/10.1007/S41939-022-00116-X/FIGURES/9>
60. Fang, L., Hong, Y.: Uncertain revised regression analysis with responses of logarithmic, square root and reciprocal transformations. *Soft. Comput.* **24**, 2655–2670 (2020). <https://doi.org/10.1007/s00500-019-03821-x>
61. Lio, W., Liu, B.: Residual and confidence interval for uncertain regression model with imprecise observations. *J. Intell. Fuzzy Syst.* **35**, 2573–2583 (2018). <https://doi.org/10.3233/JIFS-18353>
62. Lio, W., Liu, B.: Uncertain data envelopment analysis with imprecisely observed inputs and outputs. *Fuzzy Optim. Decis. Mak.* **17**, 357–373 (2018). <https://doi.org/10.1007/S10700-017-9276-X/TABLES/2>
63. Lio, W., Liu, B.: Uncertain maximum likelihood estimation with application to uncertain regression analysis. *Soft. Comput.* **24**, 9351–9360 (2020). <https://doi.org/10.1007/S00500-020-04951-3/TABLES/2>
64. Box, G.E.P., Cox, D.R.: An analysis of transformations. *J. R. Stat. Soc. Ser. B* **26**, 211–243 (1964). <https://doi.org/10.1111/J.2517-6161.1964.TB00553.X>
65. Vyas, U.B., Shah, V.A.: Optimisation based 3-dimensional polynomial regression to represent lithium-ion battery's open circuit voltage as function of state of charge and temperature. *J. Energy Storage.* **50**, 104656 (2022). <https://doi.org/10.1016/J.EST.2022.104656>
66. Raj Bukkarapu, K., Krishnasamy, A.: Support vector regression approach to optimize the biodiesel composition for improved engine performance and lower exhaust emissions. *Fuel* **348**, 128604 (2023). <https://doi.org/10.1016/J.FUEL.2023.128604>
67. Wang, P., Feng, Y., Chen, Z., Dai, Y.: Study of a hull form optimization system based on a Gaussian process regression algorithm and an adaptive sampling strategy part I: single-object optim. *Ocean Eng.* **279**, 114502 (2023). <https://doi.org/10.1016/J.OCEANENG.2023.114502>
68. Gupta, A.K., Guntuku, S.C., Desu, R.K., Balu, A.: Optimisation of turning parameters by integrating genetic algorithm with support vector regression and artificial neural networks. *Int. J. Adv. Manuf. Technol.* **77**, 331–339 (2015)
69. Sumayli, A.: Development of advanced machine learning models for optimization of methyl ester biofuel production from papaya oil: Gaussian process regression (GPR), multilayer perceptron (MLP), and K-nearest neighbor (KNN) regression models. *Arab. J. Chem.* **16**, 104833 (2023). <https://doi.org/10.1016/J.ARABJC.2023.104833>
70. Fazla, A., Aydin, M.E., Kozat, S.S.: Joint optimization of linear and nonlinear models for sequential regression. *Digit. Signal Process Rev. J.* **132**, 103802 (2022). <https://doi.org/10.1016/j.dsp.2022.103802>
71. Chandrashekar, R., Kumar, B.: Experimental investigation on energy saving potential for thermally activated buildings integrated with the active cooling system. *Energy Sour. Part A Recov. Util. Environ. Eff.* **44**, 7585–7597 (2022). <https://doi.org/10.1080/15567036.2022.2116132>
72. Grote-Ramm, W., Lanuschny, D., Lorenzen, F., Oliveira Brito, M., Schönig, F.: Continual learning for neural regression networks to cope with concept drift in industrial processes using convex optimisation. *Eng. Appl. Artif. Intell.* **120**, 105927 (2023). <https://doi.org/10.1016/J.ENGAPAI.2023.105927>
73. Yuan, H., Wang, M., Zhang, J., Zhang, Y., Lu, X.: Integrated optimization of a high-lift low-pressure turbine cascade based on dynamic support vector regression. *Aerosp. Sci. Technol.* **131**, 107986 (2022). <https://doi.org/10.1016/J.AST.2022.107986>
74. Bickel, P.J., Doksum, K.A.: An analysis of transformations revisited. *J. Am. Stat. Assoc.* **76**, 296–311 (1981). <https://doi.org/10.1080/01621459.1981.10477649>
75. Rajput, C., Kumari, S., Prajapati, V., Dinbandhu, Abhishek, K.: Experimental investigation on peel strength during ultrasonic welding of polypropylene H110MA. In: *Materials Today: Proceedings*. pp. 1302–1305. Elsevier (2020). <https://doi.org/10.1016/j.matpr.2020.02.259>
76. Peeters, J., Louarroudi, E., Bogaerts, B., Sels, S., Dirckx, J.J.J., Steenackers, G.: Active thermography setup updating for NDE: a comparative study of regression techniques and optimisation routines with high contrast parameter influences for thermal problems. *Optim. Eng.* **19**, 163–185 (2018). <https://doi.org/10.1007/S11081-017-9368-Z/TABLES/7>

Publisher's Note Springer Nature remains neutral with regard to jurisdictional claims in published maps and institutional affiliations.

Springer Nature or its licensor (e.g. a society or other partner) holds exclusive rights to this article under a publishing agreement with the author(s) or other rightsholder(s); author self-archiving of the accepted manuscript version of this article is solely governed by the terms of such publishing agreement and applicable law.